Theoretical and Applied Climatology (2020) 142:393–406
https://doi.org/10.1007/s00704-020-03312-2

ORIGINAL PAPER

Impacts of atmospheric and oceanic initial conditions on boreal summer intraseasonal oscillation forecast in the BCC model

Zhongkai Bo[1] · Xiangwen Liu[2] · Weizong Gu[1] · Anning Huang[3] · Yongjie Fang[2] · Tongwen Wu[2] · Weihua Jie[2] · Qiaoping Li[2]

Received: 10 February 2019 / Accepted: 3 July 2020 / Published online: 15 July 2020

Abstract

In this paper, we evaluate the capability of the Beijing Climate Center Climate System Model (BCC-CSM) in simulating and forecasting the boreal summer intraseasonal oscillation (BSISO), using its simulation and sub-seasonal to seasonal (S2S) hindcast results. Results show that the model can generally simulate the spatial structure of the BSISO, but give relatively weaker strength, shorter period, and faster transition of BSISO phases when compared with the observations. This partially limits the model's capability in forecasting the BSISO, with a useful skill of only 9 days. Two sets of hindcast experiments with improved atmospheric and atmosphere/ocean initial conditions (referred to as EXP1 and EXP2, respectively) are conducted to improve the BSISO forecast. The BSISO forecast skill is increased by 2 days with the optimization of atmospheric initial conditions only (EXP1), and is further increased by 1 day with the optimization of both atmospheric and oceanic initial conditions (EXP2). These changes lead to a final skill of 12 days, which is comparable to the skills of most models participated in the S2S Prediction Project. In EXP1 and EXP2, the BSISO forecast skills are improved for most initial phases, especially phases 1 and 2, denoting a better description for BSISO propagation from the tropical Indian Ocean to the western North Pacific. However, the skill is considerably low and insensitive to initial conditions for initial phase 6 and target phase 3, corresponding to the BSISO convection's active-to-break transition over the western North Pacific and BSISO convection's break-to-active transition over the tropical Indian Ocean and Maritime Continent. This prediction barrier also exists in many forecast models of the S2S Prediction Project. Our hindcast experiments with different initial conditions indicate that the remarkable model errors over the Maritime Continent and subtropical western North Pacific may largely account for the prediction barrier.

1 Introduction

The boreal summer intraseasonal oscillation (BSISO) and Madden-Julian oscillation (MJO) are two major modes of atmospheric intraseasonal variability over the tropics. Different from the MJO that is robust in the boreal winter with eastward propagation along the equator, the BSISO prevails in the boreal summer and often propagates northward over the tropical Indian Ocean to the western Pacific region. The BSISO is closely related to the weather and climate events in Asia or globally: the generation and reinforcement of tropical cyclones over the western Pacific (Wang and Zhou 2008; Kikuchi and Wang 2010), the outbreak and retreat of Asian summer monsoon (Hoyos and Webster 2007; Rajeevan et al. 2010), and the variability of extra-tropical circulation and precipitation (Ding and Wang 2007; Moon et al. 2013; Hsu et al. 2016). Therefore, the BSISO is an important target in climate modeling and forecasting.

The simulation of the BSISO, however, bears various problems, e.g., the unrealistic BSISO structure, propagation, and intensity due to the misrepresented essential model physics and air-sea coupling (Waliser et al. 2003; Fu and Wang 2004; Kim et al. 2008; Lin et al. 2008b, 2011). The state-of-the-art climate models are slowly and steadily improved in capturing the basic characteristics of the BSISO (Sabeerali et al. 2013; Fang et al. 2017), which leads to steady progresses in dynamic forecasts of the BSISO to some extent. It is found that the intraseasonal oscillation over the western Pacific

✉ Xiangwen Liu
liuxiangwen_bcc@sina.com

[1] Shandong Meteorological Bureau, Ji'nan, Shandong, China

[2] National Climate Center, and Laboratory for Climate Studies, China Meteorological Administration, Climate Model Division, 46 Zhongguancun Nandajie, Haidian District, Beijing 100081, China

[3] Nanjing University, Nanjing, Jiangsu, China

monsoon region and Indian monsoon region can be predicted with a lead time of 1–2 weeks in several climate models (Lin 2013; Suhas et al. 2013). Particularly, the European Centre for Medium-Range Weather Forecast (ECMWF) model can provide a useful skill of nearly 20 days for BSISO prediction (Lee et al. 2017). Moreover, the forecast skill can be further enhanced by multi-model ensemble forecasts (Fu et al. 2013; Neena et al. 2014; Lee et al. 2015). Although tangible progresses have been made, the intraseasonal forecasting by dynamic models is still challenging due to its remarkable sensitivity to various model settings, such as model physics, initial conditions, and air-sea coupling (Seo et al. 2005; Fu et al. 2008, 2011; Ling et al. 2014; Jie et al. 2017).

The prediction skill and predictability of the BSISO depend on the initial state of various climate components and their persistence. As a phenomenon with the time scale between synoptic weather and seasonal climate, the BSISO is remarkably affected by both the atmospheric initial conditions and underlying surface forcing. By assessing the sensitivity of BSISO forecast to atmospheric initial conditions, it is found that the forecast skills of the BSISO vary when initialized with different atmospheric reanalysis data (Fu et al. 2009, 2011). Previous study revealed that the tropical intraseasonal oscillation is sensitive to different sea surface temperature (SST) forcing, especially to that varying on the intraseasonal time scale (Pegion and Kirtman 2008). Moreover, lower boundary SST state is important for the structure and propagation of the BSISO (Liu et al. 2015). Accurate SST is thought to be essential for maintaining a higher predictability of the BSISO, and skills of the ocean-atmosphere coupled forecasts and uncoupled forecasts may be comparable under the same SST conditions (Fu et al. 2008). It is also indicated that the SST initial conditions can exert more influence on the predictability of tropical intraseasonal oscillation than the atmospheric initial conditions (Liu et al. 2017).

In recent years, the Sub-seasonal to Seasonal (S2S) Prediction Project, which provides S2S hindcasts (up to 60 days) and real-time forecast products from 11 operational and research centers, has been jointly established by the World Weather Research Program (WWRP) and the World Climate Research Program (WCRP) (Vitart et al. 2017). One of the key foci of the S2S Prediction Project is the predictability of intraseasonal variability. A series of studies have examined the performances of multiple S2S forecast models in predicting MJO, BSISO, and corresponding teleconnected influences, demonstrating remarkable differences among various models (Jie et al. 2017; Vitart 2017; Zhou et al. 2018). Results have partially shown that the Beijing Climate Center (BCC) S2S forecast model, which participates in the S2S Prediction Project, exhibits relatively low skill in MJO and BSISO forecasts. Furthermore, the BCC S2S model's limited forecast skill of the BSISO is thought to be associated with its inability to describe the physics for northward propagation of BSISO at relatively longer lead time (He et al. 2019). To reduce the deficiency in S2S forecasts, Liu et al. (2017) improved model initial conditions and enhanced MJO forecast skill by using the BCC S2S model. Therefore, it is worthwhile to investigate whether or not and to what extent the BSISO forecast can be improved by the optimization of initial conditions, and to further explore the relationship between BSISO forecasts and the reliability of model's simulation and initialization. It is also necessary to verify the validity of the optimization of initial conditions in improving S2S forecasts, and to understand different impacts of model initial conditions and internal physics on BSISO forecasts.

The rest of this paper is organized as follows. Details of the model, experiments, validation data, and methods are given in Section 2. In Section 3, we present the BSISO simulation by the BCC S2S model, and in Section 4, we show the BSISO prediction skill of the model and its sensitivity to initial conditions. Conclusions are provided in Section 5.

2 Model and data

The model used in this study is the BCC Climate System Model (BCC-CSM) version 1.2, which participates in the S2S Prediction Project (Liu et al. 2017). In the fully coupled BCC-CSM, the atmospheric component is the BCC Atmospheric General Circulation Model (AGCM) version 2, with a T106 triangular truncation in the horizontal direction and 40 layers in the vertical direction. The land component is the BCC Atmosphere and Vegetation Interaction Model version 1.0. The ocean and sea ice components are the National Oceanic and Atmospheric Administration (NOAA) Geophysical Fluid Dynamics Laboratory (GFDL) Modular Ocean Model version 4 (MOM4) and Sea Ice Simulator, respectively. The BCC model has been used in short-term climate operational prediction with reasonable skills in forecasting major climate variability at seasonal and sub-seasonal time scales (Liu et al. 2015a, 2018).

The hindcast dataset of the BCC model for the S2S Prediction Project is used in this study, and the hindcasts started on 1st, 6th, 11th, 16th, 21st, and 26th of each month during 2000–2013 are selected. Each hindcast makes a 60-day forecast integration and includes four ensemble members, with a 6-h time lag of atmospheric initial conditions for two neighboring members. For the S2S hindcasts, the atmospheric initial conditions (i.e., surface pressure, air temperature, zonal and meridional winds) are from the NCEP Reanalysis 1 (NCEP-R1; Kalnay et al. 1996), and the oceanic initial conditions (i.e., temperature and salinity) are from the multi-level temperature and salinity fields of the BCC Global Ocean Data Assimilation System (BCC-GODAS). A long-term coupled initialization run is conducted to assimilate the above observations by using nudging strategy, which produces the model

initial conditions for all hindcasts. More details about the BCC S2S hindcast experiments can be found in Liu et al. (2017).

Two additional sets of hindcast experiments are conducted to improve model's sub-seasonal forecast skill. Experiment I (EXP1) uses the similar schemes as the S2S hindcast experiments, except that the atmospheric initial conditions are improved by introducing more reliable atmospheric reanalysis data, i.e., the National Centers for Environmental Prediction (NCEP) FNL (final) Operational Model Global Tropospheric Analyses to replace the NCEP-R1. On the basis of EXP1, Experiment II (EXP2) introduces the daily Optimum Interpolation Sea Surface Temperature version 2 (OISST; Reynolds et al. 2007) to upgrade the SST initial conditions; in other words, EXP2 uses improved atmospheric and SST initial conditions. From sea surface to the depth of 30 m, a linear transition of initial fields from OISST to BCC-GODAS is adopted to keep the vertical continuity of the ocean state, and to amplify the downward impact of reliable SST initial conditions. With improved initial conditions, both EXP1 and EXP2 use the same hindcast dates as the S2S hindcast experiments. In addition, a 15-year free run without the assimilation of observations is conducted to evaluate the performance of the model itself in simulating the BSISO.

For model evaluation, we use daily outgoing longwave radiation (OLR) and wind fields from the ERA-Interim reanalysis (Dee et al. 2011), and daily SST field from the NOAA OISST (Reynolds et al. 2007). The observed daily anomalies of OLR and 850-hPa zonal wind (U850) are obtained by removing the slow annual cycle (annual mean and the first three annual harmonics of the 15-year average) and interannual variability (average of the previous 120 days). This processing method is mostly used for the verification of real-time intraseasonal forecast, although it may be limited in filtering out the interannual and long-term variability (Lyu et al. 2019a). For the results from the S2S hindcast, EXP1, and EXP2, the daily anomalies are defined by removing the lead-dependent model climatology and the mean of anomalies over the previous 120 days. To better describe the BSISO features as in Lin (2013), multivariate Empirical Orthogonal Functions (EOFs) are calculated for the observed anomalies of OLR and U850 averaged over 90°–150° E from May 1 to September 30, and the BSISO index is then defined by the two leading PCs (PC1 and PC2). The amplitude and phase angle of the BSISO are expressed as $(PC1^2 + PC2^2)^{1/2}$ and $\tan^{-1}(PC2/PC1)$, respectively. The forecasted PCs are further computed by projecting the forecasted intraseasonal anomalies onto the observed EOFs. Following the definition in Lin et al. (2008a), the bivariate anomaly correlation (BAC) and root mean square error (RMSE) between the forecasted and observed PCs are computed to measure the BSISO forecast skill.

3 BSISO characteristics in the model simulation

Given that the capability of BCC-CSM in simulating the key characteristics of BSISO is highly influential to its performance in predicting the BSISO, an uninitialized 15-year free run is conducted to show the representation of the BSISO in the model control simulation. Figure 1 presents the two leading EOF modes of daily OLR and U850 anomalies averaged over 90°–150° E. In the observation, the first EOF mode shows a strong positive center of convection anomaly near 15° N, and the second mode exhibits suppression and enhancement of convection near 10° N and 25° N, respectively. In these two modes, the maximum westerly (easterly) wind anomalies are about 5° to the south of the maximum (minimum) convection anomalies. The simulated EOF modes agree well with the observation, exhibiting a pattern correlation coefficient of 0.95 (0.91) between the observed and simulated EOF1 (EOF2) mode. The first two leading modes explain about 47% and 38% of the total variance in the observation and simulation, respectively. The results suggest that

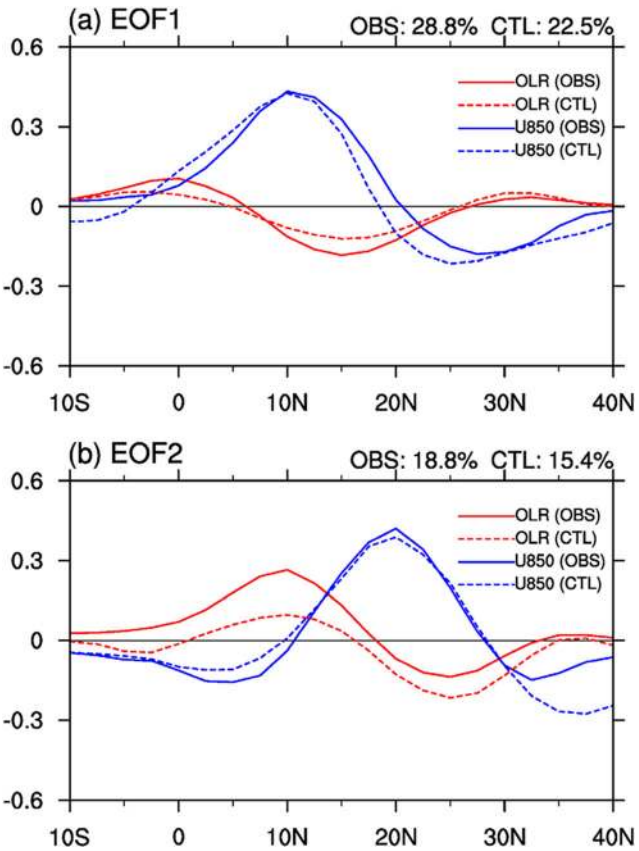

Fig. 1 Latitudinal distributions of the two leading EOF modes of combined outgoing longwave radiation and 850-hPa zonal wind in observation (solid) and control simulation (dashed). **a** EOF1; **b** EOF2. The variance explained by each mode is shown at the top right of each panel

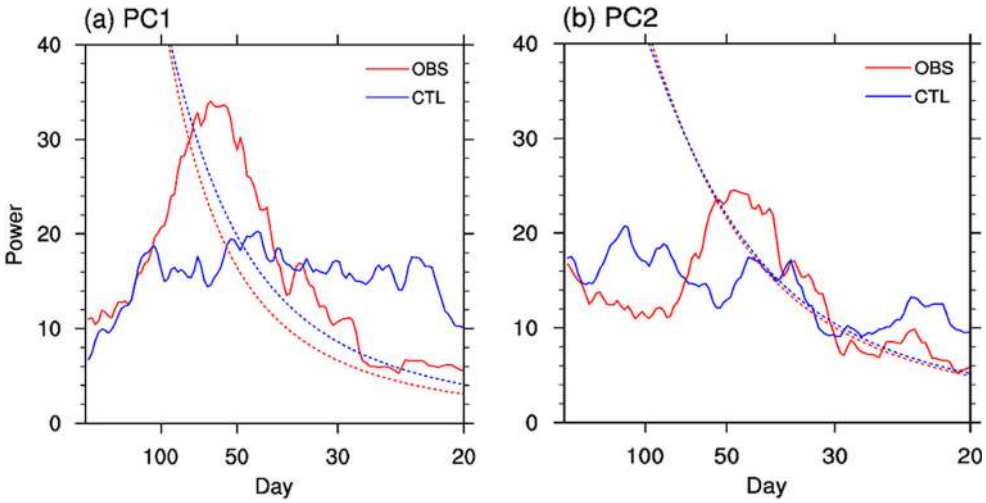

Fig. 2 Power spectra of the first two PCs of the combined EOF analysis for observations (solid red) and control simulation (solid blue). **a** PC1; **b** PC2. The red-noise spectrum at 95% confidence level is shown by dashed line

the model can reasonably reproduce the spatial structure of the observed BSISO despite some deficiencies.

Power spectral features of the first two PCs in the observation and simulation are shown in Fig. 2. The observed PC1 and PC2 are characterized by a typical intraseasonal period, showing a dominant period of 30–70 days. In the simulation, the power spectrum of PC1 has no significant peak at the intraseasonal time scale, while that of PC2 shows two bumps near the 40-day and 20-day time scales, respectively. Compared with the observation, the spectral variances are clearly underestimated at 40–100-day time scale, but are somewhat overestimated at 20–30-day time scale in the simulation, indicating that the northward-propagating BSISO is featured by a weaker strength and faster speed in the model.

Figure 3 displays the lag correlation between PC1 and PC2. In the observation, maximum (minimum) correlation between corresponding PCs is found when PC1 leads (lags) PC2 by 10 days, which are similar to the results of Lin (2013). In the model, when PC1 leads PC2, the positive correlation is basically consistent with that in the observation. However, when PC1 lags PC2, the negative correlation is obviously different from the observation, showing a lower correlation and a quicker transition with lag time. It suggests that the simulated

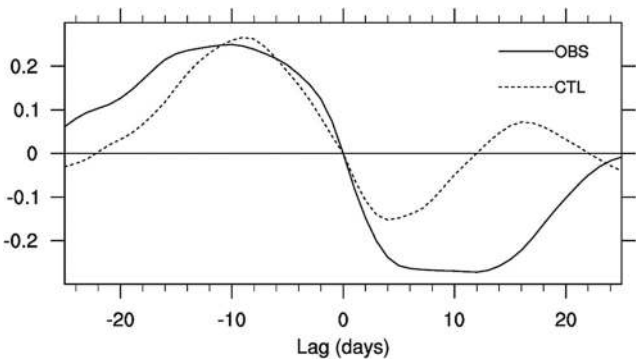

Fig. 3 Lag correlations between PC1 and PC2 in observation (solid) and control simulation (dashed)

BSISO propagates faster and shows an unreasonable phase evolution when transitioning from EOF2 to EOF1, which partially corresponds to the overestimated variance at high frequency (Fig. 2).

Composites of the OLR and 850-hPa wind anomalies for different BSISO phases are shown in Fig. 4, only BSISO events with larger-than-one amplitude being selected. In the observation, the convection initiates from the tropical Indian Ocean and Maritime Continent (phase 1), and propagates northeastward to the South China Sea as well as the tropical western Pacific (phases 2–4). With further northward propagation, the convection signal finally reaches southeastern China and the subtropical western North Pacific (phases 7–8). The model can basically reproduce the northward-propagating convection from the Indian Ocean to southeastern China, but with some apparent deficiencies. Particularly, the simulated wet anomalies at phases 1–5 and dry anomalies at phases 6–8 are considerably weaker than the observation. The underestimate is especially remarkable over the tropical Indian Ocean and Maritime Continent. In addition, from phase 6 to phase 8, a faster-than-observed propagation of convection anomaly over southeastern China and the western North Pacific and a more northward extension of convection anomaly are found, which generally agree with the results shown in Fig. 3. The weaker-than-observed BSISO variability over the tropics, especially over the equatorial Indian Ocean, is also a common deficiency for state-of-the-art climate models, including most models participated in the Coupled Model Intercomparison Project Phase 5 (Sabeerali et al. 2013).

Fig. 4 Composites of outgoing longwave radiation (*shadings*; units: W/m^2) and 850-hPa wind anomalies (*vectors*; units: m/s) for different BSISO phases in **a** observations and **b** control simulation. The number of days used to generate the composite for each phase is given at the top left of each panel. The spatial pattern correlation coefficient between observation and simulation is given at the top right of each panel

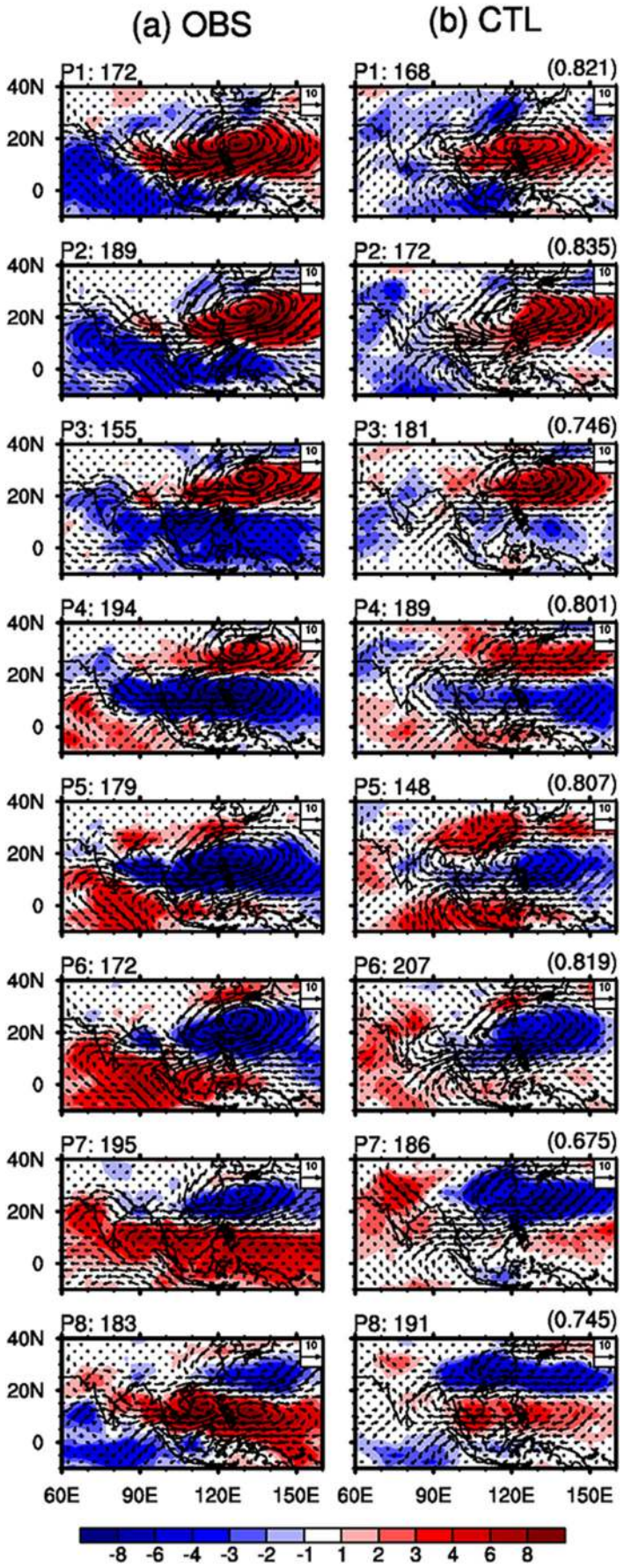
(a) OBS
(b) CTL
P1: 172
P1: 168
(0.821)
P2: 189
P2: 172
(0.835)
P3: 155
P3: 181
(0.746)
P4: 194
P4: 189
(0.801)
P5: 179
P5: 148
(0.807)
P6: 172
P6: 207
(0.819)
P7: 195
P7: 186
(0.675)
P8: 183
P8: 191
(0.745)
40N
20N
0
60E
90E
120E
150E
-8 -6 -4 -3 -2 -1 1 2 3 4 6 8

4 BSISO forecasts and impacts of improved initial conditions

Several sets of hindcast experiments are conducted using the BCC S2S forecast model. The hindcasts for the S2S Prediction Project suffer severe limitations due to the problems of imperfect model and unreliable initial conditions (Liu et al. 2017). Thus, EXP1 and EXP2 are carried out to improve the model forecast skill by upgrading the atmospheric and both atmospheric and SST initial conditions, respectively.

Figure 5 shows the forecast skills of SST and U850 in the first 2 weeks of forecasts, and the differences of skill among different hindcasts. In the first week, with optimized atmospheric and ocean initial conditions in the model, remarkable forecast skills of SST and U850 are found over most areas in EXP2 (Fig. 5a1, b1). In the second week, the forecast skill of SST remains high over the extra-tropics but relatively lower over the tropical Indian Ocean and western Pacific (Fig. 5a5), while that of U850 is considerably low over most areas (Fig. 5b5), denoting an obviously higher predictability of SST than that of atmospheric circulations. During the first 2 weeks of forecasts, SST forecast skill is little increased over the tropics from the S2S hindcasts to EXP1 (Fig. 5a2, a6), while U850 forecast skill is enhanced over many regions, especially over the southeastern Indian Ocean and southwestern Pacific (Fig. 5b2, b6). Moreover, during the first 2 weeks, the SST forecast skill is remarkably improved over most areas in EXP2 over EXP1 (Fig. 5a4, a8), while the U850 forecast

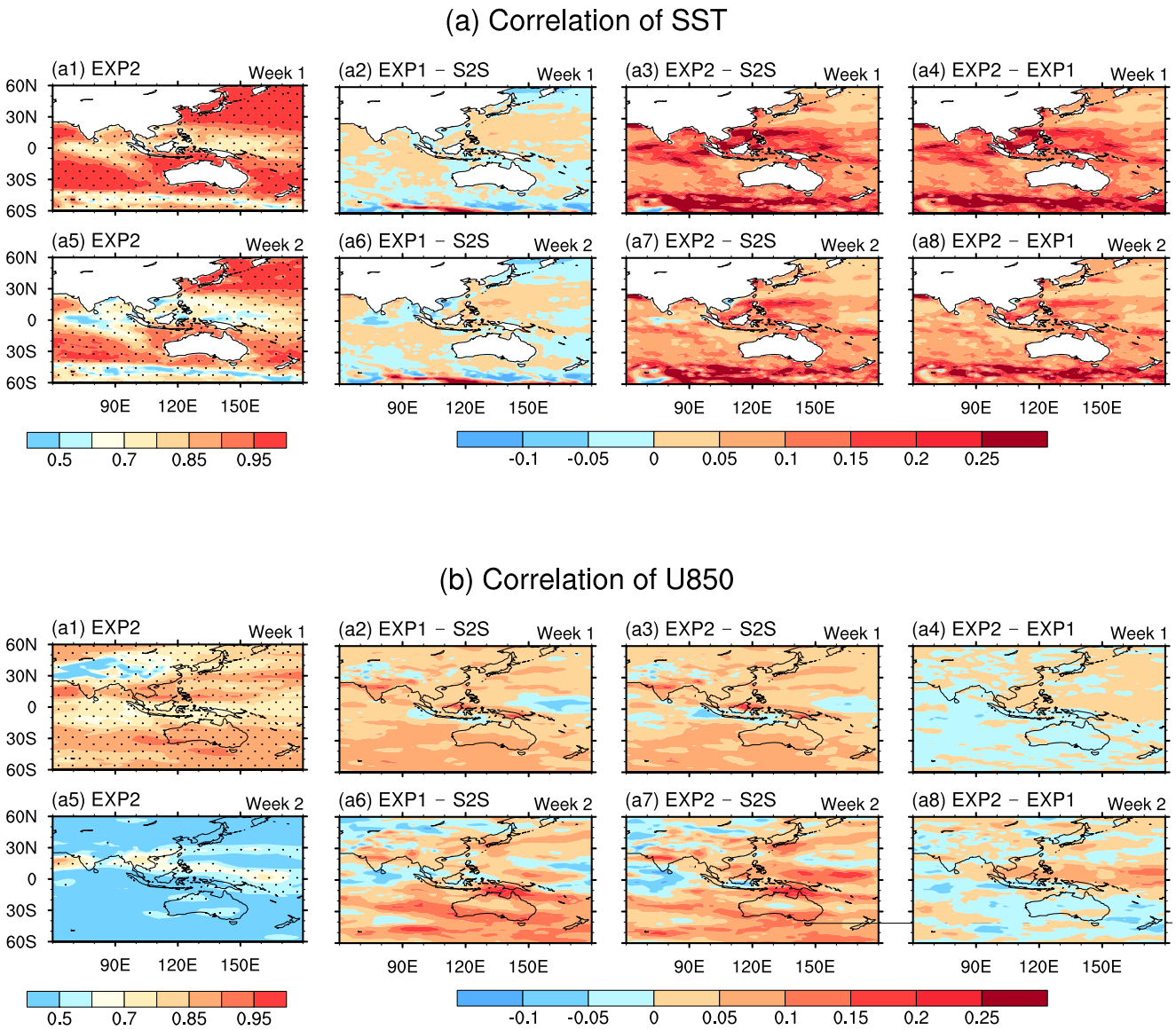

Fig. 5 Anomaly correlations between observations and forecasts for **a1**, **a5** SST and **b1**, **b5** 850-hPa zonal wind averaged during the first and second weeks of forecast. Also shown are the differences of correlation skills **a2**, **a6**, **b2**, **b6** between EXP1 and S2S hindcasts; **a3**, **a7**, **b3**, **b7** between EXP2 and S2S hindcasts; and **a4**, **a8**, **b4**, **b8** between EXP2 and EXP1. Stippling represents the statistical significance of correlation above the 99% confidence level

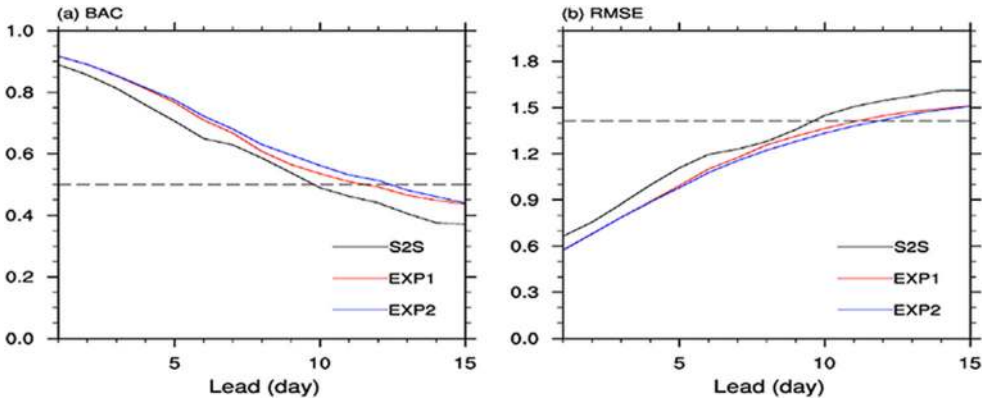

Fig. 6 **a** Bivariate anomaly correlation and **b** root mean square error between observations and forecasts in the S2S hindcasts (*black*), EXP1 (*blue*), and EXP2 (*red*). The *horizontal dashed line* represents the values of 0.5 and 1.414 in **a** and **b**, respectively

skill basically remains unchanged in the first week, but is slightly improved over the tropical western Pacific in the second week (Fig. 5b4, b8). It indicates that for climate variability forecasts over the western Pacific, the improvement of atmospheric initial conditions exerts more impacts on atmospheric circulation forecasts rather than on SST forecasts. The optimization of SST initial conditions can impact SST forecasts, and meanwhile affect the atmospheric circulation forecasts beyond the lead time of 1 week.

Figure 6 shows the overall forecast skills of the BSISO in various hindcast experiments. The BAC and RMSE between forecasted and observed PCs are computed to measure the BSISO forecast skill. Taken BAC = 0.5 as the threshold of useful skill, the forecast skill of about 9 days is found in the S2S hindcasts, and the skill increases to 11 and 12 days in EXP1 and EXP2, respectively (Fig. 6a). Also, taken the RMSE = 1.414 as the upper limit of useful skill, similar improvements are seen as those of BAC (Fig. 6b). The forecast skills in the experiments with improved atmospheric and oceanic initial conditions are comparable to those in several state-of-the-art models (Lee and Wang 2016; Jie et al. 2017). These results reveal a 3-day increase of forecast skill from the S2S hindcasts to EXP2, demonstrating the impacts of optimized atmospheric and oceanic initial conditions. It confirms the importance of accurate initial conditions in BSISO forecasts revealed by previous studies (Fu et al. 2008, 2009; Lee et al. 2015). In addition, from EXP1 to EXP2, the BSISO forecast skill remains almost unchanged in the first week but is improved in the second week. This corresponds to the skill difference of U850 over the tropical western Pacific between the two sets of hindcasts as shown in Fig. 5, indicating the gradually emerging impacts of ocean initial conditions beyond the lead time of 1 week.

The sensitivity of forecast skill to initial conditions may vary with different definitions of the BSISO. The BSISO index defined by Lin (2013) is used in this study, namely, the zonal average of OLR and U850 over 90°–150° E is examined. By using another BSISO index (Lee et al. 2013), the

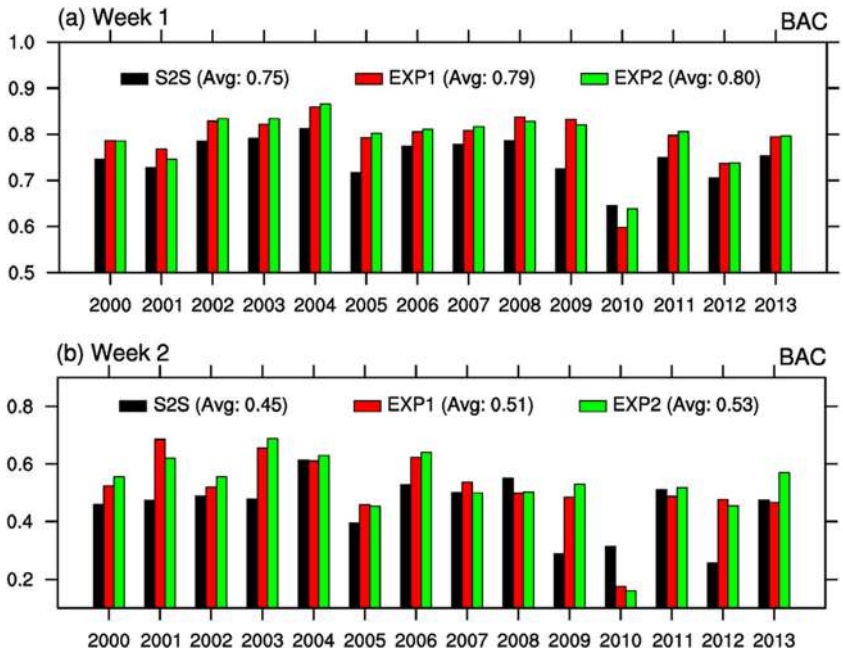

Fig. 7 BSISO forecast skill (bivariate anomaly correlation) in **a** the first week and **b** second week of forecast in each year during 2000–2013 for the S2S hindcasts (*black*), EXP1 (*red*), and EXP2 (*green*). The values in parentheses show the skill averages of all years

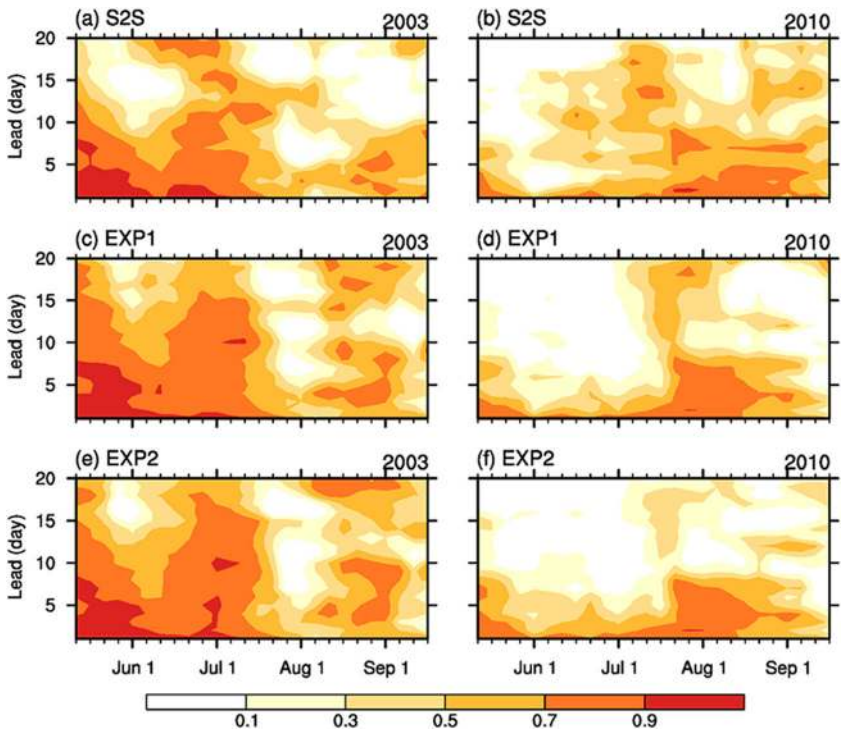

Fig. 8 Bivariate correlation between observations and forecasts as a function of lead time and calendar date. Skills are computed by using experiments within a monthly window centered on each forecast date starting from May to September in 2003 and 2010 for **a**, **b** S2S hindcasts; **c**, **d** EXP1; and **e**, **f** EXP2

two-dimensional OLR, U850, and 850-hPa meridional wind over the region (40°–160° E, 10° S–40° N) are analyzed. Results show that the forecast skill is about 9 days in the S2S hindcasts, which increases to 10 and 12 days in EXP1 and EXP2, respectively (figures omitted). Although the former index, which shows a smoother spatial feature, is more easily to be depicted by the model than the latter index, comparable skills are found for both indexes. Comparison with the results shown in Jie et al. (2017) indicates that the forecast skill of EXP2 is comparable to those of the models in the S2S Prediction Project.

Figure 7 shows the interannual variation of BSISO forecast skill in the first 2 weeks of forecasts during 2000–2013. From the S2S hindcasts to EXP1 and EXP2, the overall forecast skill of the BSISO shows a slight improvement in both the first and second weeks, indicating the positive effects of the optimization of initial conditions. Meanwhile, the forecast skill exhibits significant interannual variation. For example, the forecast skill was extremely low in 2010, while it was relatively higher in 2003 and 2004 than that in the other years. From the S2S hindcasts to EXP1 and EXP2, the features of monthly evolution of forecast skill (Fig. 8) reveal that the useful skill increases to 2–3 weeks during May–August 2003 several times. However, relatively low skills remain unchanged in most summers, and especially low values of less than 5 days are found during May–July 2010. The failure of initialization optimization in 2010 may be caused by the obviously low predictability of the BSISO itself, in addition to the uncertainty in the interaction between model errors and initial errors. The above skill differences might be closely related to the interannual variation of BSISO amplitude (Liu et al. 2015b), given that the forecasts by various models are always more skillful for BSISO events with stronger amplitude than those with weaker amplitude (Lee et al. 2015; Jie et al. 2017). In this study, we find that clear interannual differences are also featured by different skill degrees for the three hindcast sets, and different amplitude of skill declines from the first week to the second week in those years, altogether revealing complicated impacts of atmospheric and oceanic initializations.

Figure 9 illustrates the dependence of BSISO forecast skill on initial/target phases and lead times in various hindcasts. We again take BAC = 0.5 as the threshold of useful skill. In the S2S hindcasts, the forecast skills range from 8 to 12 days for different initial phases, with the minimum for initial phase 6 and relatively high skills near initial phases 8 and 1 (Fig. 9a). It indicates that the BSISO is easy to predict when it initiates from the equatorial Indian Ocean, but difficult to forecast when it starts from the South China Sea and western North Pacific. From the S2S hindcasts to EXP1, the forecast skills are obviously improved for many initial phases except phases 4–6 (Fig. 9b). Moreover, the forecast skills from initial phases 1 and 2 are further improved in EXP2, with the maximum skill near the 18-day lead time. However, useful skills at the lead time less than 10 days for forecasts near initial phase 6 are hardly changed (Fig. 9c). Besides, the forecast skill varies with target phase, with relatively higher values near target phases 5–8 and lower values near target phases 3–4,

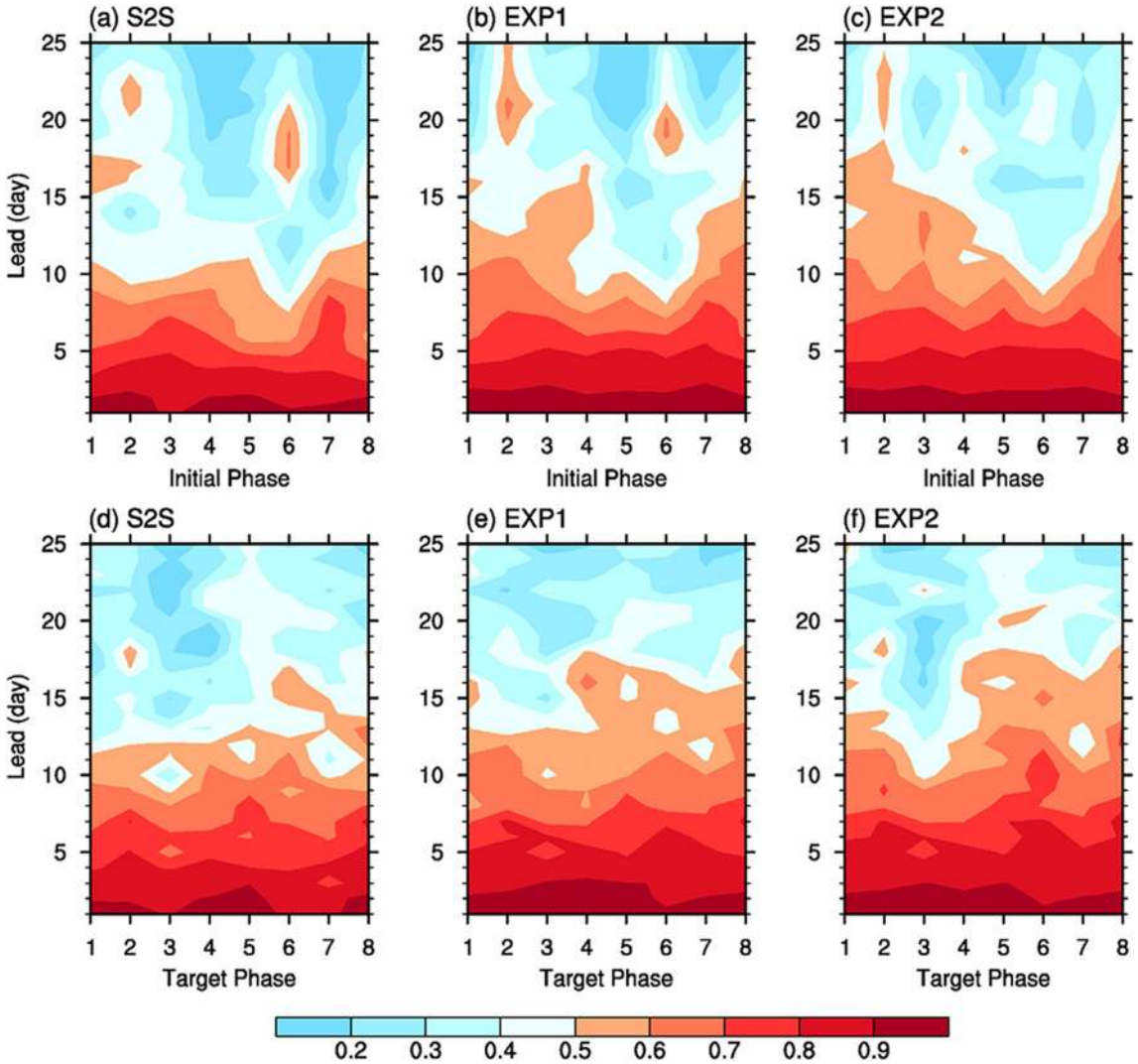

Fig. 9 BSISO forecast skill (bivariate anomaly correlation) as a function of lead time and BSISO phase for strong initial or target cases (amplitude > 1.0) in **a**, **d** S2S hindcasts; **b**, **e** EXP1; and **c**, **f** EXP2. The forecast skill is stratified by initial phase (top panels) and target phase (bottom panels)

corresponding to skill peaks near initial phases 8, 1, and 2, and to skill valley near initial phase 6 (Fig. 9e, f). The results indicate that the BSISO is difficult to forecast when the convection signal dissipates over the western North Pacific and reinitiates from the Indian Ocean and Maritime Continent, but can be skillfully predicted when the convection signal propagates from the Indian Ocean into the western North Pacific in both EXP1 and EXP2. Previous study has shown that the most significant forecast skills of the BSISO near initial phases 1 and 8 are found in two thirds of the models in the Intraseasonal Variability Hindcast Experiment (ISVHE) Project (Lee et al. 2015), whereas the lowest forecast skills of the BSISO mostly appear around target phases 3–5 for 10 models in the S2S Project (Jie et al. 2017). Although the forecast skill and its sensitivity to initial and target phases are always model-dependent, these results to some extent suggest a common prediction barrier of the BSISO as depicted in many of the state-of-the-art climate forecast models.

Given the most significant skill enhancement for initial phase 2 and the smallest improvement for initial phase 6, Fig. 10 shows the time–latitude composites of forecasted OLR and U850 anomalies for these two initial phases. For initial phase 2, the enhanced convection anomaly in the observation propagates northward from the equator to the South China Sea, and the suppressed convection anomaly propagates from the South China Sea to the Northwest Pacific (Fig. 10a). In the S2S hindcasts, the intensity of convection anomaly is apparently underestimated, and the northward propagation of convection shows a faster-than-observed decay with lead time (Fig. 10c). The intensity and propagation of convection anomalies in EXP1 and EXP2 are obviously improved due to the improvements of initial conditions (Fig. 10e, g). For initial phase 6, the negative convection anomaly in the observation propagates from the equator to the South China Sea, while the positive convection anomaly propagates over the South China Sea (Fig. 10b). In the S2S

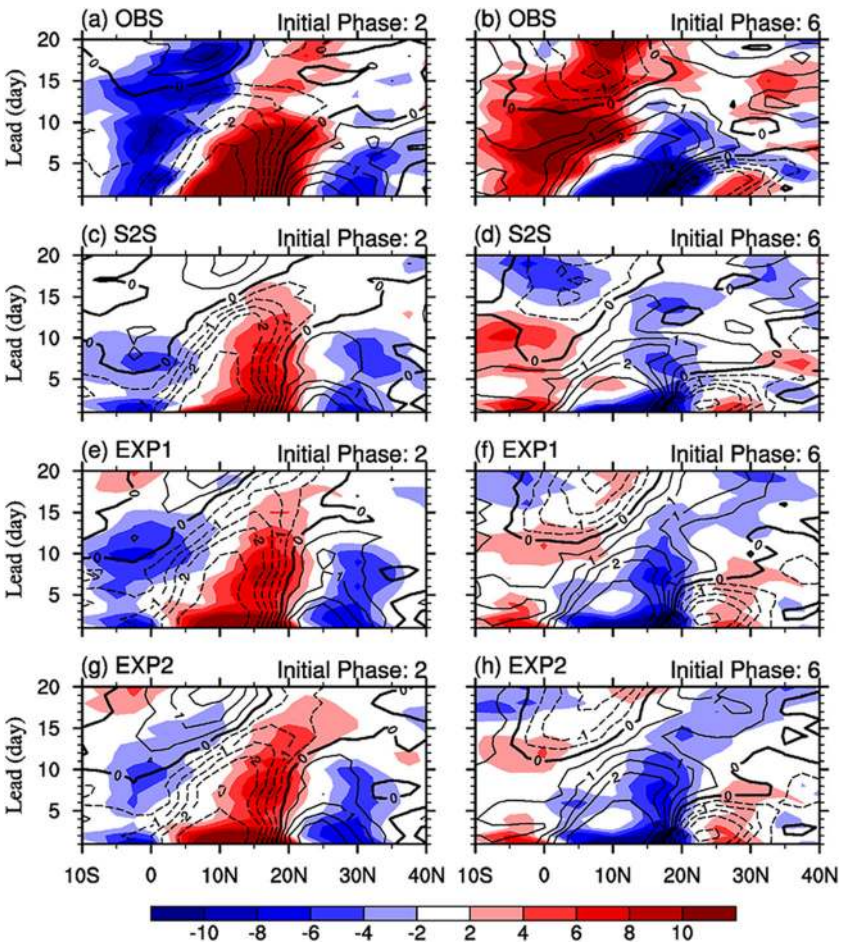

Fig. 10 Time–latitude composites of outgoing longwave radiation (*shadings*; units: W/m^2) and 850-hPa zonal wind (*contours*; units: m/s) anomalies for the BSISO initial phase 2 (*left column*) and phase 6 (*right column*) in **a**, **b** observations; **c**, **d** S2S hindcasts; **e**, **f** EXP1; and **g**, **h** EXP2

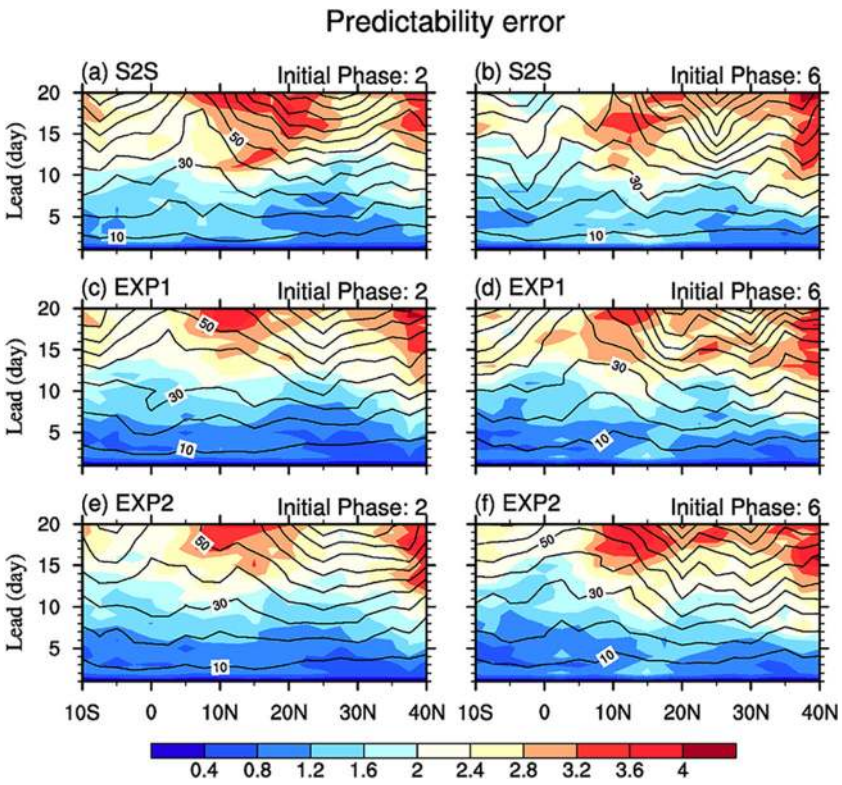

Fig. 11 Time–latitude diagram of predictability error of outgoing longwave radiation (*contours*; units: W/m^2) and 850-hPa zonal wind (*shadings*; units: m/s) anomalies for the BSISO initial phase 2 (*left column*) and phase 6 (*right column*) in **a**, **b** S2S hindcasts; **c**, **d** EXP1; and **e**, **f** EXP2

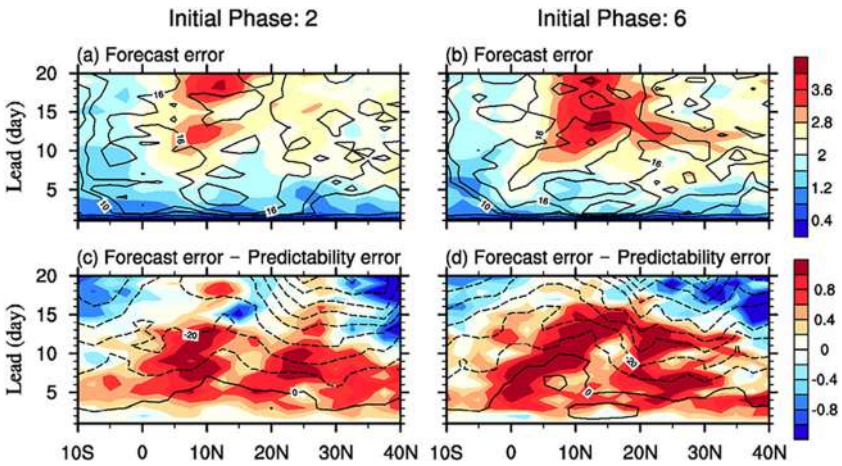

Fig. 12 Time–latitude diagram of **a**, **b** forecast error and **c**, **d** differences between forecast error and predictability error of outgoing longwave radiation anomalies (*contours*; units: W/m^2) and 850-hPa zonal wind anomalies (*shadings*; units: m/s) for the BSISO initial phase 2 (*left column*) and phase 6 (*right column*) in EXP2

hindcasts, the intensity of convection anomaly is apparently weaker than the observation, and the convection enhancement shows a longer duration over the South China Sea with a more northward propagation over the subtropical areas (Fig. 10d). In EXP1 and EXP2 (Fig. 10f, h), although the magnitude of convection enhancement is improved at short lead time to certain extent, the abovementioned deficiencies generally maintain, indicating that improved initial conditions have no obviously positive effect on the forecast of BSISO propagation from initial phase 6. It is suggested that the intrinsic model problem to sustain dry phases near the equator, as shown in Fig. 4, might have contributed to the unskillful forecasts of the BSISO from phase 6 significantly.

For the two initial phases mentioned above, the variations of predictability errors and forecast errors of U850 and OLR with lead time are shown in Figs. 11 and 12. The forecast error is defined as the RMSE between forecasts and observations, and the predictability error is estimated by computing the RMSE between each perturbed member and the control member and then averaging the results of the three ensemble subsamples. These definitions are similar to the forecast skill and predictability measured by BAC in Kim et al. (2014). Based on a perfect-model assumption, the predictability error is used to measure the error features caused by the uncertainty of initial conditions, and its difference with the forecast error can partially represent the impacts of model errors. For predictability errors of the forecasts (Fig. 11), the differences among ensemble members are always small at short lead time, and gradually increase with lead time, thus showing large spreads at longer lead time. The increase of predictability errors due to the uncertainty of initial conditions is obviously faster in the S2S hindcasts than those in EXP1 and EXP2 within 10-day lead time, denoting more reliable initial conditions adopted by the latter two. The predictability errors become remarkable near 15° N and 40° N beyond the lead time of 10–15 days, whereas the error magnitude is generally comparable among various forecasts, suggesting that an upper limit of potential predictability may be reached. The variations of forecast errors show different features (Fig. 12). In EXP2, the forecasts from initial phases 2 and 6 are both featured by relatively remarkable forecast errors over the tropical and subtropical western Pacific beyond 1-week lead time, with a maximum center near 10–20° N at 10–20-day lead time (Fig. 12a, b). Especially, the error magnitude for forecasts from initial phase 2 is obviously smaller than that from initial phase 6. The differences between forecast errors and predictability errors (Fig. 12c, d) further indicate that associated with the northward propagation of the BSISO, the model error evolves with lead time and latitude, presenting a much larger amplitude and longer duration for forecasts from initial phase 6 than from initial phase 2. Particularly, two maximum error centers are located over the Maritime Continent and the subtropical western North Pacific, respectively. These results agree with those shown in Figs. 1, 2, 3, and 4, in which a significantly underestimated convection near the Maritime Continent and a clearly faster-than-observed propagation of the BSISO with a gradual subsiding convection anomaly over the western North Pacific are simulated. All these factors lead to a rapid decline of forecast skill for the propagation of the BSISO beyond the 10-day lead time from initial phase 6. It demonstrates that the model deficiency other than unreliable initial conditions should largely account for the abovementioned BSISO prediction barrier.

5 Conclusions

In this study, we evaluated the capability of the BCC model in simulating and forecasting the BSISO. We also explored the impacts of improved initial conditions on BSISO prediction skill by the model. Our main findings are summarized here.

The model simulates a faster-than-observed propagation of the BSISO from the equatorial Indian Ocean to southeastern China and the subtropical western North Pacific, with an apparently underestimate in the intensity of convection over the Indian Ocean and western equatorial Pacific. The useful forecast skill of the BSISO is about 9 days in the S2S hindcasts, which is increased to 12 days in EXP2 due to the improved atmospheric and oceanic initial conditions. The improved

forecast skill in EXP2 is comparable to the skills in several state-of-the-art dynamic forecast models (Lee and Wang 2016; Jie et al. 2017). Note that from EXP1 to EXP2, the BSISO forecast skill remains almost unchanged in the first week of forecast, but is slightly improved in the second week, indicating the gradually emerging influence of the ocean initial conditions beyond the lead time of 1 week.

The BSISO forecast skill significantly depends on initial and target phases. In the S2S hindcasts, the model shows higher skills in initial phases 8 and 1 when the convection anomaly develops over the tropical Indian Ocean, and shows lower skill in initial phase 6 when the convection anomaly is initially located over the South China Sea. From the S2S hindcasts to EXP1 and EXP2, the overall forecast skill is enhanced for most initial phases except phase 6 due to the improved initial conditions. In EXP1 and EXP2, the propagation from the tropical Indian Ocean and Maritime Continent to the South China Sea is obviously improved, but the propagation from southern China and the subtropical western North Pacific is still difficult to predict. Further exploration reveals that the rapid increase of model errors over the Maritime Continent and the subtropical western North Pacific near initial phase 6 is responsible for the low forecast skill of the BSISO and its insensitivity to the change of initial conditions.

The above results reveal that the BSISO forecast skill can be improved with the introduction of more accurate atmospheric and oceanic initial conditions. However, there are still some obvious deficiencies in the BSISO prediction due to the imperfection of the model itself. On the one hand, the faster-than-observed propagation is predicted in various hindcasts by the model, which is attributed to the short periodicity of the BSISO in the model as shown in Fig. 2. Given that the slower-than-observed northward propagation is also found in other models, it is suggested that this feature is highly model-dependent (Wang et al. 2009; Fu et al. 2013). On the other hand, the model shows apparent difficulties in predicting the BSISO propagation from southern China and the subtropical western North Pacific, which also occurs in most models in the S2S Project (Jie et al. 2017). In this case, the convection over the western North Pacific is in an active-to-break transition, whereas the convection from the tropical Indian Ocean and the South Asian monsoon region to the Maritime Continent is in a break-to-active transition. Several studies have shown that the break-to-active transition is less predictable than the active-to-break transition of monsoon over the South Asia region (Goswami and Xavier 2003; Fu et al. 2013), which is consistent with the finding of this study. Therefore, for the prediction barrier of the BSISO during its northward propagation, which is a common deficiency in many climate models, more efforts should be made in the future for further improving the forecast skill of the BSISO.

In addition to the BSISO, the MJO is also one of the targets for improving the S2S forecast in this study, given that the MJO is a dominant mode of intraseasonal atmospheric variability and exerts remarkable modulations on the tropical and extra-tropical weather and climate events (e.g., Kikuchi and Wang 2010; He et al. 2011; Moon et al. 2013; Hsu et al. 2016; Lyu et al. 2019b). Liu et al. (2017) showed that the useful skill of MJO forecast by the BCC model was about 16 days in the S2S hindcasts, and increased to 18 days by optimizing atmospheric initial conditions and 22 days by optimizing both atmospheric and oceanic initial conditions. This indicates that the BSISO and MJO can both be well predicted by the model with updated initialization schemes, although these two climate phenomena differ in active period and propagation feature. At the second phase of the S2S Project, a BCC model version with enhanced resolution and upgraded initialization schemes will be used to further improve sub-seasonal forecast.

Funding information This study was jointly supported by the National Key R&D Program of China (Grant 2016YFA0602100), the National Natural Science Foundation of China (Grant 41675090), and Shandong Meteorological Bureau Research Program of China (Grant 2017sdqxm03).

References

Dee DP, Uppala SM, Simmons AJ, Berrisford P, Poli P, Kobayashi S, Andrae U, Balmaseda MA, Balsamo G, Bauer P, Bechtold P, Beljaars ACM, van de Berg L, Bidlot J, Bormann N, Delsol C, Dragani R, Fuentes M, Geer AJ, Haimberger L, Healy SB, Hersbach H, Hólm EV, Isaksen L, Kållberg P, Köhler M, Matricardi M, McNally AP, M

Ding Q, Wang B (2007) Intraseasonal teleconnection between the summer Eurasian wave train and the Indian monsoon. J Clim 20(15): 3751–3767

Fang Y, Wu P, Mizielinski MS, Roberts MJ, Wu T, Li B, Vidale PL, Demory ME, Schiemann R (2017) High-resolution simulation of the boreal summer intraseasonal oscillation in met Office unified model. Q J R Meteorol Soc 143(702):362–373

Fu X, Wang B (2004) Differences of boreal summer intraseasonal oscillations simulated in an Atmosphere–Ocean coupled model and an atmosphere-only model. J Clim 17(6):1263–1271

Fu X, Yang B, Bao Q, Wang B (2008) Sea surface temperature feedback extends the predictability of tropical intraseasonal oscillation. Mon Weather Rev 136(2):577–597

Fu X, Wang B, Bao Q, Liu P, Lee J-Y (2009) Impacts of initial conditions on monsoon intraseasonal forecasting. Geophys Res Lett 36(8): 134–150

Fu X, Wang B, Lee J-Y, Wang W, Gao L (2011) Sensitivity of dynamical intraseasonal prediction skills to different initial conditions. Mon Weather Rev 139(8):2572–2592

Fu X, Lee J-Y, Wang B, Wang W, Vitart F (2013) Intraseasonal forecasting of the Asian summer monsoon in four operational and research models. J Clim 26(12):4186–4203

Goswami BN, Xavier PK (2003) Potential predictability and extended range prediction of Indian summer monsoon breaks. Geophys Res Lett 30(18):1966

He J, Lin H, Wu Z (2011) Another look at influences of the Madden–Julian oscillation on the wintertime East Asian weather. J Geophys Res Atmos 116(D3)

He Z, Hsu P, Liu X, Wu T, Gao Y (2019) Factors limiting the forecast skill of the boreal summer intraseasonal oscillation in a subseasonal-to-seasonal model. Adv Atmos Sci 36(1):104–118

Hoyos CD, Webster PJ (2007) The role of intraseasonal variability in the nature of Asian monsoon precipitation. J Clim 20(17):4402–4424

Hsu P, Lee J-Y, Ha KJ (2016) Influence of boreal summer intraseasonal oscillation on rainfall extremes in southern China. Int J Climatol 36(3):1403–1412

Jie W, Vitart F, Wu T, Liu X (2017) Simulations of Asian summer monsoon in the Sub-seasonal to Seasonal Prediction Project (S2S) database. Q J R Meteorol Soc 143(706):2282–2295

Kalnay E, Kanamitsu M, Kistler R, Collins W, Deaven D, Gandin L, Iredell M, Saha S, White G, Woollen J, Zhu Y, Leetmaa A, Reynolds R, Chelliah M, Ebisuzaki W, Higgins W, Janowiak J, Mo KC, Ropelewski C, Wang J, Jenne R, Joseph D (1996) The NCEP/NCAR 40-year reanalysis project. Bull Am Meteorol Soc 77(3):437–471

Kikuchi K, Wang B (2010) Formation of tropical cyclones in the Northern Indian Ocean associated with two types of tropical intraseasonal oscillation modes. J Meteorol Soc Japan 88(3):475–496

Kim H-M, Kang I-S, Wang B, Lee J-Y (2008) Interannual variations of the boreal summer intraseasonal variability predicted by ten atmosphere-ocean coupled models. Clim Dyn 30(5):485–496

Kim H-M, Webster PJ, Toma VE, Kim D (2014) Predictability and prediction skill of the MJO in two operational forecasting systems. J Clim 27(14):5364–5378

Lee S-S, Wang B (2016) Regional boreal summer intraseasonal oscillation over Indian Ocean and Western Pacific: comparison and predictability study. Clim Dyn 46(7–8):2213–2229

Lee J-Y, Wang B, Wheeler MC, Fu X, Waliser DE, Kang I-S (2013) Real-time multivariate indices for the boreal summer intraseasonal oscillation over the Asian summer monsoon region. Clim Dyn 40(1–2):493–509

Lee S-S, Wang B, Waliser DE, Neena JM, Lee J-Y (2015) Predictability and prediction skill of the boreal summer intraseasonal oscillation in the Intraseasonal Variability Hindcast Experiment. Clim Dyn 45(7–8):2123–2135

Lee S-S, Moon J-Y, Wang B, Kim H-J (2017) Subseasonal prediction of extreme precipitation over Asia: boreal summer intraseasonal oscillation perspective. J Clim 30(8):2849–2865

Lin H (2013) Monitoring and predicting the intraseasonal variability of the East Asian-Western North Pacific summer monsoon. Mon Weather Rev 141(3):1124–1138

Lin H, Brunet G, Derome J (2008a) Forecast skill of the Madden–Julian oscillation in two Canadian atmospheric models. Mon Weather Rev 136(11):4130–4149

Lin JL, Weickman KM, Kiladis GN, Mapes BE, Schubert SD, Suarez MJ, Bacmeister JT, Lee MI (2008b) Subseasonal variability associated with Asian summer monsoon simulated by 14 IPCC AR4 coupled GCMs. J Clim 21(18):4541–4567

Lin A, Li T, Fu X, Luo J-J, Masumoto Y (2011) Effects of air-sea coupling on the boreal summer intraseasonal oscillations over the tropical Indian Ocean. Clim Dyn 37(11–12):2303–2322

Ling J, Bauer P, Bechtold P, Beljaars A, Forbes R, Vitart F, Ulate M, Zhang C (2014) Global versus local MJO forecast skill of the ECMWF model during DYNAMO. Mon Weather Rev 142(6):2228–2247

Liu F, Huang G, Yan M (2015) Role of SST meridional structure in coupling the Kelvin and Rossby waves of the intraseasonal oscillation. Theor Appl Climatol 121(3–4):623–629

Liu X, Wu T, Yang S, Jie W, Nie S, Li Q, Cheng Y, Liang X (2015a) Performance of the seasonal forecasting of the Asian summer monsoon by BCC_CSM1.1(m). Adv Atmos Sci 32(8):1156–1172

Liu X, Yang S, Li J, Jie W, Huang L, Gu W (2015b) Subseasonal predictions of regional summer monsoon rainfalls over tropical Asian oceans and land. J Clim 28:9583–9605

Liu X, Wu T, Yang S, Li T, Jie W, Zhang L, Wang Z, Liang X, Li Q, Cheng Y, Ren H, Fang Y, Nie S (2017) MJO prediction using the sub-seasonal to seasonal forecast model of Beijing Climate Center. Clim Dyn 48(9–10):3283–3307

Liu X, Li W, Wu T et al (2018) Validity of parameter optimization in improving MJO simulation and prediction using the sub-seasonal to seasonal forecast model of Beijing Climate Center. Clim Dyn 52(7–8):3823–3843

Lyu M, Jiang X, Wu Z (2019a) A cautionary note on the long–term trend in activity of the Madden–Julian oscillation during the past decades. Geophys Res Lett 46(23):14063–14071

Lyu M, Wu Z, Shi X, Wen M (2019b) Distinct impacts of the MJO and the NAO on cold wave amplitude in China. Q J R Meteorol Soc 145:1617–1635

Moon J-Y, Wang B, Ha K-J, Lee J-Y (2013) Teleconnections associated with Northern Hemisphere summer monsoon intraseasonal oscillation. Clim Dyn 40(11–12):2761–2774

Neena JM, Jiang X, Waliser D, Lee J-Y, Wang B (2014) Eastern Pacific intraseasonal variability: a predictability perspective. J Clim 27(23):8869–8883

Pegion K, Kirtman BP (2008) The impact of air-sea interactions on the predictability of the tropical intraseasonal oscillation. J Clim 21(22):5870–5886

Rajeevan M, Gadgil S, Bhate J (2010) Active and break spells of the Indian summer monsoon. J Earth Syst Sci 119(3):229–247

Reynolds RW, Smith TM, Liu C, Chelton DB, Casey KS, Schlax MG (2007) Daily high-resolution-blended analyses for sea surface temperature. J Clim 20(22):5473–5496

Sabeerali CT, Dandi AR, Dhakate A, Salunke K, Mahapatra S, Rao SA (2013) Simulation of boreal summer intraseasonal oscillations in the latest CMIP5 coupled GCMs. J Geophys Res Atmos 118(10):4401–4420

Seo K-H, Schemm J-KE, Jones C, Moorthi S (2005) Forecast skill of the tropical intraseasonal oscillation in the NCEP GFS dynamical extended range forecasts. Clim Dyn 25(2–3):265–284

Suhas E, Neena JM, Goswami BN (2013) An Indian monsoon intraseasonal oscillations (MISO) index for real time monitoring and forecast verification. Clim Dyn 40(11–12):2605–2616

Vitart F (2017) Madden–Julian oscillation prediction and teleconnections in the S2S database. Q J R Meteor Soc 143(706):2210–2220

Vitart F, Ardilouze C, Bonet A, Brookshaw A, Chen M, Codorean C, Déqué M, Ferranti L, Fucile E, Fuentes M, Hendon H, Hodgson J, Kang HS, Kumar A, Lin H, Liu G, Liu X, Malguzzi P, Mallas I, Manoussakis M, Mastrangelo D, MacLachlan C, McLean P, Minami A, Mladek R, Nakazawa T, Najm S, Nie Y, Rixen M, Robertson AW, Ruti P, Sun C, Takaya Y, Tolstykh M, Venuti F, Waliser D, Woolnough S, Wu T, Won DJ, Xiao H, Zaripov R, Zhang L (2017) The Sub-seasonal to Seasonal (S2S) Prediction Project database. Bull Am Meteorol Soc 98(1):163–173

Waliser DE, Jin K, Kang I-S, Stern WF, Schubert SD, Wu MLC, Lau KM, Lee MI, Krishnamurthy V, Kitoh A, Meehl GA, Galin VY, Satyan V, Mandke SK, Wu G, Liu Y, Park CK (2003) AGCM

simulations of intraseasonal variability associated with the Asian summer monsoon. Clim Dyn 21(5–6):423–446

Wang B, Zhou X (2008) Climate variation and prediction of rapid intensification in tropical cyclones in the western North Pacific. Meteorog Atmos Phys 99(1–2):1–16

Wang W, Chen M, Kumar A (2009) Impacts of ocean surface on the northward propagation of the boreal summer intraseasonal oscillation in the NCEP climate forecast system. J Clim 22(24):6561–6576

Zhou Y, Yang B, Chen H, Zhang Y, Huang A, La M (2018) Effects of the Madden–Julian oscillation on 2-m air temperature prediction over China during boreal winter in the S2S database. Clim Dyn 52:6671–6689